LSB FLOW CONDITIONING USING SPANWISE MODULATED DISTURBANCES: HWA AND TOMO-PIV MEASUREMENTS

J. W. Kurelek
Mechanical and Materials Eng.
Queen's University
Kingston ON, Canada
john.kurelek@queensu.ca

T. Michelis*, M. Kotsonis†
Aerospace Eng.
Delft University of Technology
Delft, The Netherlands
t.michelis@tudelft.nl*
m.kotsonis@tudelt.nl†

S. Yarusevych
Mechanical and Mechatronics Eng.
University of Waterloo
Waterloo ON, Canada
syarus@uwaterloo.ca

ABSTRACT

This work examines conditioning a laminar separation bubble (LSB) using spanwise modulated disturbances. The investigations is carried out in a series of wind tunnel tests, with the LSB formed over a flat plate subject to an adverse pressure gradient. Building from previous work (Kurelek *et al.*, 2023), a new approach to produce velocity disturbances of a controllable spanwise wavelength is used to study the growth of spanwise modes in the LSB, with measurements performed using hot-wire anemometry (HWA) and tomographic particle image velocimetry (tomo-PIV). From the HWA measurements, small amplitude disturbances at the frequency of the LSB's primary Kelvin-Helmholtz instability are identified upstream of the LSB, which undergo convective amplification downstream of the mean separation point. When forced at this fundamental frequency in a two-dimensional manner, disturbance growth is almost entirely confined to the normal (2D) mode. When spanwise modulated forcing is applied, a distinct spanwise mode emerges in the disturbance profile, which is also convectively amplified. These findings point to the flow's instability to both normal and oblique disturbance waves, which can superimpose to form the experimentally measured disturbance profiles. The small amplitude disturbances tracked through the fore portion of the LSB are found to manifest in the shear layer vortices, imparting a spanwise wavelength, if present, in the vortex filaments. This can lead to significant dislocations developing across the span of the filaments, where the streamwise forward sections tilt up and away from the wall, leading to further vortex stretching by the mean shear.

INTRODUCTION

Laminar separation bubbles are common in low Reynolds number flows, typically characterized by a chord-based Reynolds number of less than 5×10^5. Relevant engineering applications include low-pressure turbomachinery, small-to-medium scale wind turbines, micro and unmanned aerial vehicles, and larger aircraft operating at low speed or high altitude. The main impediment to performance in these applications is boundary layer separation, which brings losses severe enough that a dedicated class of low Reynolds number airfoils exists, where separation mitigation is the primary design consideration (Carmichael, 1981). Still, flow separation is typical to these airfoils, as the boundary layer on the suction side often remains laminar into the adverse pressure gradient region. If separation occurs, an unstable separated shear layer is formed where a relatively rapid amplification of perturbations leads to vortex shedding and an enhancement of momentum exchange that can cause the flow to reattach to the surface in a mean sense. In such cases, a closed region of recirculating fluid forms, *i.e.*, an LSB, the very presence of which can be detrimental to performance, causing loss in the lift-to-drag ratio, and/or an increase in noise emissions (*e.g.*, Arcondoulis *et al.*, 2010). Further, LSBs leave the flow in an unstable configuration, as only slight changes in the environment or operating conditions can suddenly leave the LSB unable to reattach, leading to abrupt stall (Gaster, 1967).

The present work is motivated by the possibility of gaining control authority over an LSB, specifically through three-dimensional or spanwise modulated forcing actions, since doing so could serve to address the aforementioned negative performance impacts. Typically, control authority over LSBs is achieved using spanwise-uniform flow control techniques that target the shear layer vortices directly (*e.g.*, Yarusevych & Kotsonis, 2017). This type of forcing locks the vortex shedding process to the excitation frequency, advances vortex formation upstream, and increases the spanwise coherence of the structures (Kurelek *et al.*, 2018). Such an approach is effective at inducing mean reattachment on a stalled airfoil (and thus forming an LSB), or reducing the size of an existing LSB. However, energizing and increasing the spanwise coherence of the LSB shear layer vortices can be problematic, as doing so can increase the unsteady loads or noise amplitudes generated on an airfoil. Particularly problematic is the case of airfoil self-noise – a phenomenon where sharp tones are produced by the passage of strongly periodic and spanwise-coherent structures over the airfoil trailing edge (Desquesnes *et al.*, 2007). Thus, a technique that simultaneously gains control authority over an LSB but also reduces the spanwise coherence of its shear layer vortices could be highly desirable in such circumstances.

Developing such a technique is predicated on LSB flows showing sensitivity to three-dimensional disturbances. Along this line of inquiry, theoretical predictions employing approximated LSB velocity profiles and Linear Stability Theory (LST) have shown that the relevant growth rates are always highest for the normal mode (*i.e.*, for a zero spanwise wavenumber, $k_z = 0$) (Dovgal *et al.*, 1994). These findings have been supported by both experimental (Michelis *et al.*, 2018; Rist & Augustin, 2006) and Direction Numerical Simulation (DNS) (Marxen *et al.*, 2003, 2004) studies, and are aligned with the preferential amplification of two-dimensional modes by the Kelvin-Helmholtz instability of separated and free shear layers (Michalke, 1964). As noted by Dovgal *et al.* (1994), the growth rate of spanwise modes is lower, yet comparable, to that of the normal modes in LSBs, while the amplification rates of three-dimensional modes in attached boundary layers can be up to ten times that of the two-dimensional Tollmien-Schlichting waves. Thus, when considering an LSB in isolation, as is the case in analytical approximations and simulations with prescribed in-flow conditions, three-dimensional disturbances appear to be of little significance (Marxen *et al.*, 2004).

However, when the continuous stability spectrum is considered, beginning from the upstream boundary layer and into an LSB, there is evidence that three-dimensional disturbance development can play a significant role. In a DNS study, Rist & Augustin (2006) found that weakly oblique instability waves grow at comparable rates to the two-dimensional normal mode, leading to an earlier onset of turbulent breakdown when oblique wave angles are less than 30°. A wave angle of 30° corresponds to a spanwise-to-streamwise wavelength ratio 1.73. They also reported the introduction of these oblique waves caused a spanwise staggering of the LSB vortex shedding process, leading to a peak and valley distribution in the mean flow field quantities. Experimental studies of the same nature are relatively scarce due to the difficulty in implementing a reliable spanwise modulated forcing technique, which is then compounded by the need for three-dimensional flow field measurements. A notable exception is Michelis *et al.* (2018), who noted spanwise deformations in naturally developing LSBs. There, a spanwise-to-streamwise wavelength ratio of 1.94 was found, while applying two-dimensional forcing almost entirely eliminated the spanwise modulations. As a result, a model for vortex deformations in LSBs was proposed based on the ratio of amplitudes between normal and oblique disturbances present in the attached boundary layer upstream.

The present study builds off of the authors' previous work, where a novel approach to producing three-dimensional flow disturbances of a controllable spanwise wavelength was introduced and validated (Kurelek *et al.*, 2023). Here, the same technique is used as a diagnostic tool in studying the growth of spanwise disturbance modes in an LSB, which is examined in the fore and aft portion of the LSB using HWA and tomo-PIV measurements, respectively.

EXPERIMENTAL SETUP

Experiments were conducted in the Anechoic Vertical Low Turbulence Wind Tunnel (A-Tunnel) at Delft University of Technology. This is a closed-circuit wind tunnel with a free-stream uniformity within $\pm 1\%$ and a turbulence intensity of 0.09%. A schematic of the setup is provided in Fig. 1, where the test section cross-sectional area was configured to 500×500 mm, and an LSB was formed over a $1000 \times 500 \times 20$ mm flat plate through the application of an adverse pressure gradient. The free-stream velocity was set to $U_\infty = 5.75\,\mathrm{m\,s^{-1}}$, corresponding to a Reynolds number of $Re_{\delta_s^*} = 750$ based on the displacement thickness at separation when the flow is not forced ($\delta_s^* = 2.0$ mm). Throughout this report, U_∞ and δ_s^* are used as the velocity and length scale for non-dimensionalization, respectively. To simplify the notation, all dimensional quantities are typeset as uppercase and are accompanied with units (*e.g.*, $U_1 = 3.45\,\mathrm{m\,s^{-1}}$, $\Lambda_z = 50$ mm), and all non-dimensional quantities are typeset as lowercase (*e.g.*, $u_1 = U_1/U_\infty = 0.60$, $\lambda_z = \Lambda_z/\delta_s^* = 25$). In discussing disturbance development, the notation $(k_x, k_z) = (m, \pm n)$ is used to specify spatial Fourier modes, where k_x and k_z are the streamwise and spanwise wavenumbers, respectively, and m and n are integer multiples of the fundamental streamwise and spanwise wavenumbers, $k_{x_0} = 0.08$ and $k_{z_0} = 0.04$.

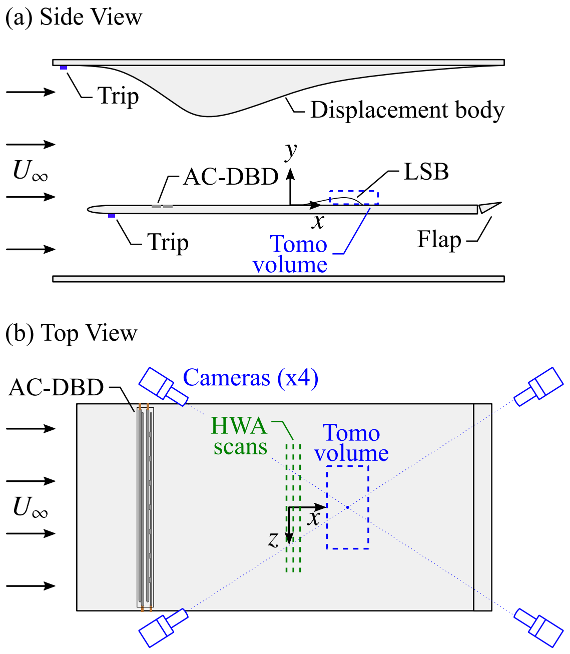

Figure 1. Experimental setup for HWA and tomo-PIV measurements within the LSB. Coordinate system origin is located on the top surface of the plate, at the mid-span location where the flow separates in unforced conditions.

Alternating current, dielectric barrier discharge (AC-DBD) plasma actuators were used to introduce controlled disturbances into the flow, upstream of the LSB (Fig. 1). A full description of the technique and employed configuration is provided in Kurelek *et al.* (2023). In short, the technique is capable of producing flow disturbances of a controllable frequency and spanwise wavelength while holding total input momentum constant via superposition of the outputs of two plasma actuators arranged in streamwise succession. Three cases are considered: (i) the natural/unforced flow, (ii) two-dimensional forcing, and (iii) three-dimensional forcing with a spanwise wavelength of $\lambda_z = 25$, chosen to achieve a wavelength ratio of $\lambda_z/\lambda_{x0} = 2$. All disturbances were produced using the same plasma actuator parameters: peak-to-peak voltage, $V_{\mathrm{pp}} = 6$ kV, carrier frequency, $F_{\mathrm{c}} = 5$ kHz, and modulation frequency, $F_{\mathrm{m}} = 133$ Hz. The latter was selected to target the primary Kelvin-Helmholtz instability of the LSB shear layer.

Velocity measurements were conducted using HWA and tomo-PIV to resolve disturbance development near the mean separation point and three-dimensional flow development in the LSB aft, respectively. Phase-averaging of both the HWA and tomo-PIV measurements was enabled by referencing the plasma forcing signal.

The HWA measurements were performed in spanwise scans at wall-normal heights equal to local displacement thickness, with the probe kept at least 2 mm from the wall to avoid near-zero velocities, surface conduction and rectification errors. A Dantec 55P15 boundary layer probe was used, which was held at a 10° to the plate surface by a rigid, streamwise-aligned sting mounted to a 3-axis traverse system. Uncertainty in the probe position was estimated to be less than 0.06 mm. Sampling was performed at 51.2 kHz for 5 s, collecting 2.56×10^5 samples per location. The sensor was operated by a TSI IFA-300 constant temperature bridge, with the bridge outputs digitized by a 24-bit National Instruments acquisition module. Calibrations were performed against a reference Pitot-static probe and repeated on a daily basis, during which the ambient temperature typically drifted by 0.5 °C and never exceeded a change of 1 °C. A fourth order polynomial fit to 17 calibration points spanning $0 \leq u \leq 2$ was used, with the distribution of points weighted to the lower end of the velocity range. Taking into account the probe geometry, temperature effects, calibration method, and level of the measured velocity fluctuations, the uncertainty in the HWA measurements is estimated to be less than 3% of U_∞ within the range of measured velocities ($0.60 \leq u \leq 0.78$).

The tomo-PIV system consisted of a Quantel EverGreen 200 mJ/pulse Nd:YAG laser synchronized with four PCO sCMOS 5.5MP cameras through a LaVision timing unit. Each camera was equipped with a Scheimpflug adapter and a 200 mm focal length macro lens set to $f_\# = 11$. The laser beam was collimated using a set of spherical lenses, then expanded via a cylindrical lens to illuminate a $69 \times 7.6 \times 120$ mm ($X \times Y \times Z$) volume. Light attenuation effects at the volume boundaries were mitigated by a knife edge filter. An initial physical calibration was performed by imaging a 3D calibration target, and then refined using volume self-calibration (Wieneke, 2008) to a final calibration uncertainty of less than ± 0.1px. Double-frame particle images were acquired using a frame separation time of 100 µs, keeping particle displacements under 17 px. The volume reconstruction was performed using the SMART algorithm (Atkinson & Soria, 2009), yielding a final interrogation volume of $1499 \times 165 \times 2605$ vox. Volume displacements were estimated iteratively using cubic windows with 75% overlap and a final size of 20 vox, yielding $300 \times 33 \times 521$ vectors in the volume and a vector pitch of 0.23 mm in all three coordinate directions. Given the complexity of the tomo-PIV technique, producing a reliable estimate of the measurement uncertainty remains challenging. Here, the reliability of the tomographic results is established through comparison with equivalent planar PIV measurements (from Kurelek *et al.*, 2023), since a more robust estimate of uncertainty is available for the latter. Based on this approach, the uncertainty in the tomo-PIV mean quantities is estimated on the order of 3.5% of U_∞ for $y > 0.5$.

RESULTS

Figure 2 presents an overview of the flow development within the unforced LSB through time-averaged velocity statistics, while also providing an opportunity to compare the tomo-PIV results to prior planar PIV measurements from the same setup (Kurelek *et al.*, 2023). In Fig. 2(a), a region of reverse flow ($\overline{u} < 0$) is present near the wall between $0 \leq x \leq 50$, indicating the presence of time-averaged flow separation and reattachment, and thus an LSB. The outline of the LSB is identified by the mean dividing streamline (solid black line in Fig. 2), which forms a closed contour with the surface within which the time-averaged streamwise mass flux is zero (O'Meara & Mueller, 1987). The displacement thickness, δ^* is also plotted (dashed black line) and follows a similar profile to the dividing streamline; steadily increasing downstream of separation and then decreasing to a local minimum downstream of reattachment. The spanwise HWA scans were taken at four streamwise locations, $x = -4.50, 1.75, 8.00$ and 14.25, each at the local value of δ^*, with these locations indicated in Fig. 2 by the red × markers.

Comparing the planar and tomographic PIV results in Fig. 2, the overall agreement is very good, with the mean streamwise velocity profiles in the aft portion of the LSB showing excellent agreement (Fig. 2(a)). Only slight discrepancies are seen in the mean wall-normal velocity profiles (Fig. 2(b)), which are attributed to the significantly lower magnitudes and thus relatively higher uncertainties for this velocity component. Good agreement is also found in the velocity fluctuations, as seen for u'_{rms} and v'_{rms} in Figs. 2(c) and (d), respectively. Slight discrepancies are apparent at the most upstream and downstream stations, $x = 32$ and 62, respectively, which results from the relatively low and high amplitude fluctuations at these stations, respectively, in addition to the significant spatial filtering applied by the tomographic processing algorithm. However, all noted discrepancies are relatively minor, and the overall excellent agreement establishes the reliability of the tomo-PIV measurements to a level of uncertainty that is greater than, but similar to, that of the planar PIV, determined to be 3.5% of U_∞ for $y > 0.5$ (Kurelek *et al.*, 2023).

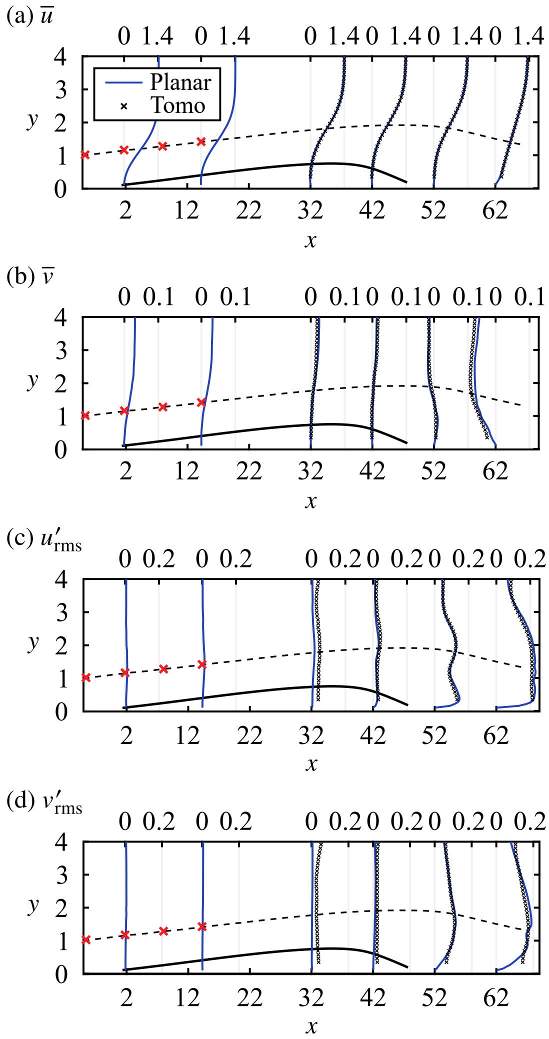

Figure 2. Velocity statistics in the unforced LSB at $z = 0$, compared between planar (from Kurelek *et al.*, 2023) and current tomographic measurements. Solid and dashed black lines indicate the mean dividing streamline and displacement thickness, respectively, estimated from the planar PIV. Red × markers indicate locations of the spanwise HWA scans.

Disturbance development in the fore portion of the LSB is examined via the HWA measurements, taken in spanwise scans at the locations indicated in Fig. 2. To isolate the fundamental perturbation mode, the streamwise velocity fluctuations are band-pass filtered about the forcing modulation frequency, $F_{\mathrm{m}} = 133$ Hz, and then phase-averaged with respect to the forcing cycling. Since no phase information is available

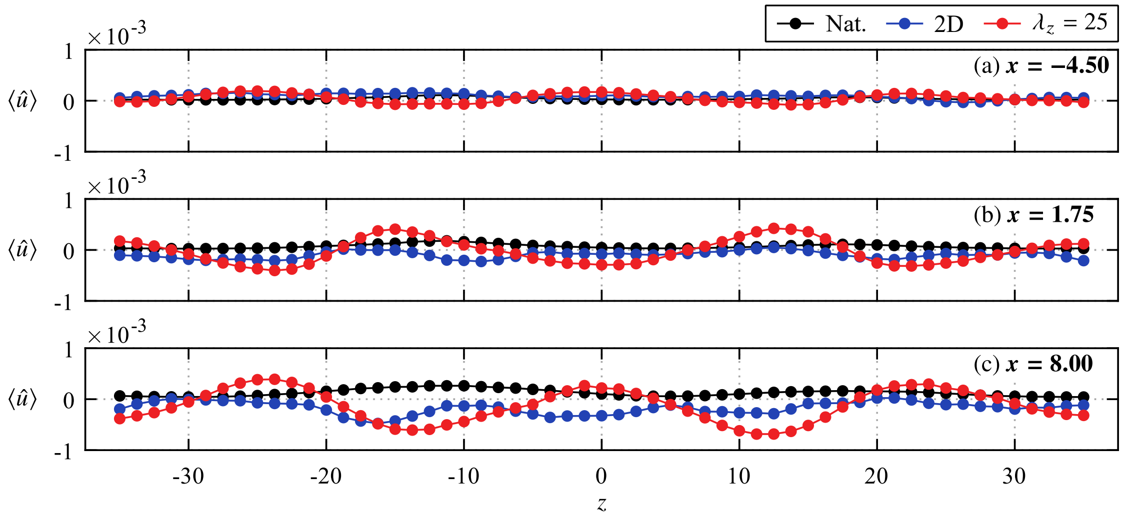

Figure 3. Phase-averaged streamwise perturbations of the fundamental (forcing) frequency, $\langle\hat{u}\rangle$, at phase $\theta = 0$. Measured via HWA at several streamwise stations near the mean LSB separation point ($x_s = 0$).

for the natural case, root-mean-square values are calculated in place of phase-averages. The results are plotted in Fig. 3, with the 2D and $\lambda_z = 25$ cases shown at the same phase, $\theta = 0$. At the most upstream station (Fig. 3(a)), disturbance amplitudes are low and comparable for all cases. Due to convective amplification, disturbance amplitudes increase at the downstream stations. Examining Fig. 3(c), primarily negative velocity amplitudes are seen for the 2D and $\lambda_z = 25$ forcing cases, indicating that the convective disturbances are within their negative half-cycle, while the amplitude of the natural disturbance wave is rendered positive by taking the root-mean-square. On an absolute basis, the observed convective amplification of the 2D and $\lambda_z = 25$ disturbances indicates that there is a preferred amplification of the artificial disturbances.

Comparing the 2D and $\lambda_z = 25$ case in Fig. 3(c), the effect of the spanwise modulated forcing is readily apparent. While both waves have similar spanwise-averaged, *i.e.*, normal mode $(1,0)$, amplitudes, the $\lambda_z = 25$ case shows a distinct spanwise modulation at the intended wavelength. Thus, significant fluctuating energy is contained within this mode, *i.e.*, the first spanwise mode $(1,\pm1)$. It is well established that the Kelvin-Helmholtz instability is responsible for amplification of the $(1,0)$ mode in LSBs (Rist & Augustin, 2006; Marxen & Henningson, 2011), while here experimental evidence is presented for a mechanism by which spanwise disturbances modes are amplified in LSBs.

The streamwise evolution of disturbances depicted in Fig. 3 consists of both the $(1,0)$ and $(1,\pm1)$ modes, which are influenced by the forcing. These constituent components are quantified through a spatial Fourier analysis of the HWA data. A spatial Fast Fourier Transform is applied to the signals presented in Fig. 3, producing wavenumber spectra at each streamwise station. The full spanwise extent of the measurement domain is used, consisting of 57 measurements (padded with zero values to 64) over an extent of $70z$, yielding a wavenumber resolution $0.31k_z$, which is coarse but sufficient to delineate the $(1,0)$ and $(1,\pm1)$ modes. The result is presented in Fig. 4. Note that due to the convective nature of the disturbances, the amplitudes of the spatial Fourier modes change with phase at a given streamwise position. Therefore, the wavenumber spectra at each x position are averaged across all phases, allowing for the growth of the modes to be tracked with downstream development.

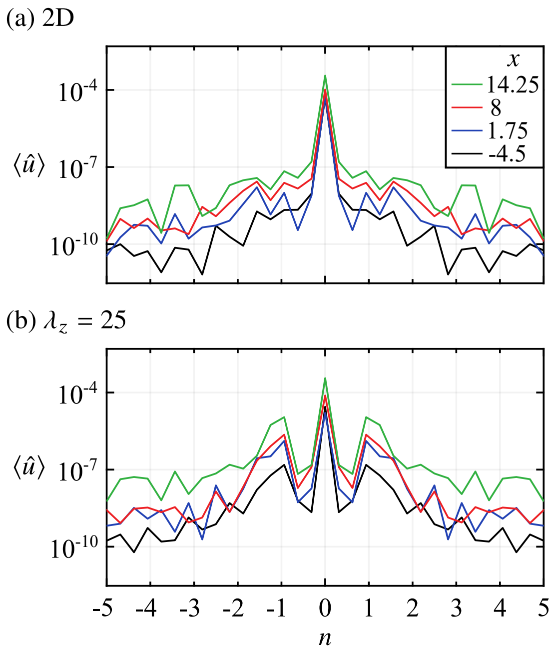

Figure 4. Streamwise evolution of spatial Fourier modes of the fundamental streamwise wavenumber ($m = 1$).

From Fig. 4(a), disturbance growth in the fore portion of the LSB is almost entirely confined to the normal mode when the flow is forced with 2D perturbations, as the modal amplitude of $(1,0)$ exceeds that of any spanwise mode by at least three orders of magnitude. This is consistent with the disturbances depicted in Fig. 3 for the 2D case, which are spanwise uniform and, while not shown for brevity, oscillate in a spanwise uniform manner through the phases of the forcing cycle. For the $\lambda_z = 25$ forcing case (Fig. 4(b)), peaks are observed at both $(1,0)$ and $(1,\pm1)$, with both modes growing in amplitude as the disturbances convect downstream. The amplification of both of these modes is supported by previous linear stability analyses of LSBs (Rist & Augustin, 2006; Michelis *et al.*, 2018), which have found unstable growth rates near mean separation for both normal and spanwise modes. Notably, the growth rates of the spanwise modes are reported to be compa-

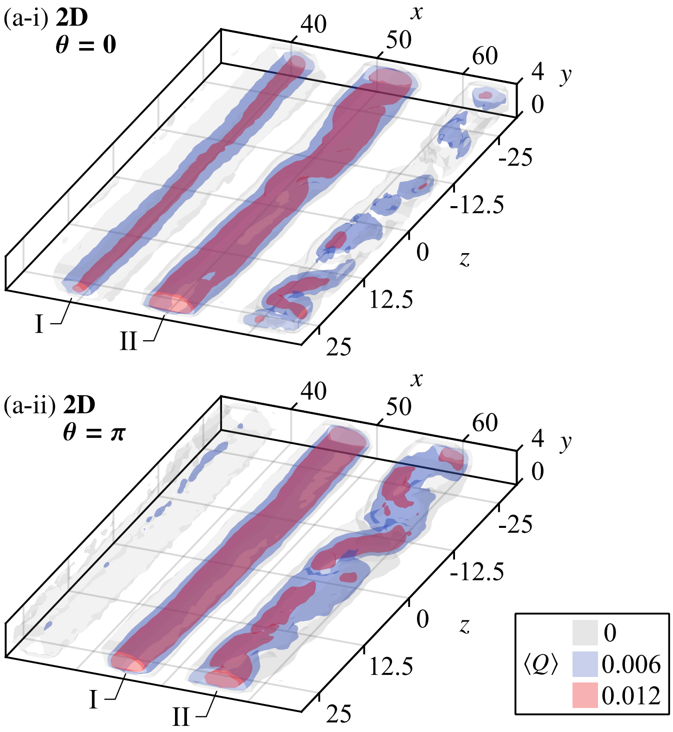

Figure 5. Phase-averaged flow development in the aft of the LSB, visualized via iso-surfaces of the Q-criterion (Hunt *et al.*, 1988).

rable to that of the normal modes for oblique wave angles less than $\vartheta = 27°$ (Michelis *et al.*, 2018) ($\vartheta = \tan^{-1}(k_z/k_x)$). In the current experiment, the ratio of the forcing/fundamental spanwise and streamwise wavenumbers is $1/2$, yielding an oblique wave angle of $\vartheta = 26.6°$.

From Fig. 4, the ratio of amplitudes between the $(1,0)$ and $(1,\pm 1)$ modes remain relatively constant across the three most downstream stations for both the 2D and $\lambda_z = 25$ cases, at $5 \times 10^3 : 1$ and $30 : 1$, respectively. The relative contributions of the modes to the total fluctuating energy can also be quantified through integration of the wavenumber spectra. Using the most downstream station ($x = 14.25$) and $0.62k_z$ wide bands centred on the modes, the $(1,0)$ mode comprises 99.8% of the total fluctuating energy under 2D forcing, while under $\lambda_z = 25$ forcing, the $(1,0)$ and $(1,\pm 1)$ modes account for 90.8% and 7.2% of the total energy, respectively. For the 2D case, the prevalence of the normal mode both in terms of amplitude and allocation of fluctuating energy reinforces that disturbance growth, and thus the transition process in this region, is driven entirely by the $(1,0)$ mode. This is not the case for the $\lambda_z = 25$ forcing, where the 2D mode still dominates, but to a lesser degree, as an appreciable portion of energy is contained, and critically, sustained by the flow in the $(1,\pm 1)$ mode.

A mechanism by which spanwise undulatory velocity disturbances can manifest in LSBs has been proposed by Michelis *et al.* (2018), with their modelled disturbances (see their Fig. 19) showing a striking similarity to those reported here (Fig. 3). They demonstrate that unstable normal and oblique disturbances can exist in the attached boundary layer upstream of an LSB, where through a symmetric resonant triad (Craik, 1971; Zelman & Maslennikova, 1993), they can superimpose to form a spanwise undulatory wave front. Critical to this superposition is the amplitude ratio between the normal and oblique modes, reporting highly distorted and nominally two-dimensional spanwise flow states at amplitude ratios of 3.3 : 1 and 40 : 1, respectively.

Focus now shifts to the vortex dynamics in the LSB aft under the influence of different forcing scenarios. Figure 5 presents phase-averaged flow development in this region, visualized through iso-surfaces of the Q-criterion (Hunt *et al.*, 1988). The results highlight the differences in spatial structure and development of the shear layer vortices under the different forcing scenarios. Notably, the most upstream vortices in Fig. 5(a-i) and (b-i), labelled I and III, are largely similar, showing strong spanwise uniformity; however, a spanwise undulation in vortex III is discernible and matches the $\lambda_z = 25$ forcing wavelength. Tracking this structure downstream to Fig. 5(b-ii), the undulation intensifies leading to dislocations that begin to develop in vortex III at $z = \pm 12.5$. These dislocations are most readily apparent in vortex IV in Fig. 5(b-i) and (b-ii), as this structure appears highly distorted across the span but still maintains an undulatory shape with a spanwise wavelength of $\lambda_z = 25$. Thus, the small amplitude disturbances tracked through the fore portion of the LSB (Fig. 3) are found to manifest in the shear layer vortices as a spanwise undulation of a matching wavelength. In contrast, 2D forcing leads to vortices that maintain a strong spanwise coherence and persists to farther downstream stations. This is most evident by comparing vortices II and IV between Fig. 5(a-i) and (b-i), respectively, where the former maintains a high degree of spanwise coherence while the latter has developed significant spanwise dislocations.

Disturbance amplitudes in the aft portion of the LSB ($x > 50$) are relatively high, with u'_{rms} and v'_{rms} approaching nearly 20% of U_∞ (Fig. 2). Therefore, the assumptions made in the fore portion of the LSB – that disturbances remain small in amplitude, of a single frequency, and do not interact – no longer apply. Instead an assessment of the vortex dynamics is more appropriate, where a link back to the upstream disturbance development can be drawn. Examining vortex IV in Fig. 5(b-ii), the streamwise forward sections of the filament, *e.g.*, at $z = 0$, are located farther from the wall than the sections that lag behind. This is highlighted in Fig. 6, where a cross-flow view of vortex IV is provided, and its core is estimated through local maxima detected in $\langle Q \rangle$. This lift-up of the streamwise forward segments could be the result of the initial small-amplitude spanwise perturbations present in flow, since a vortex filament of such topology would self-induce a net rotational motion. This rotation would lift up and push down the streamwise forward and rearward sections of the filament, respectively, which coupled with the strong wall-normal velocity gradient, would lead to an continual intensification of vortex stretching.

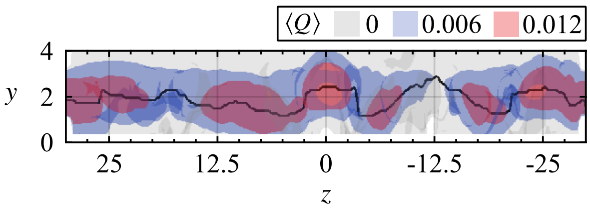

Figure 6. Cross-flow view of vortex IV from Fig. 5(b-ii). Black solid line estimates the core of the vortex.

CONCLUSIONS

The conditioning of flow development in a laminar separation bubble (LSB) was explored using spanwise modulated disturbances, with the investigations carried out in a series of wind tunnel tests. The LSB was formed over a flat plate subject to an adverse pressure gradient, and new approach to producing velocity disturbances of a controllable spanwise wavelength (Kurelek *et al.*, 2023) was used to study the growth of spanwise modes in the LSB. Measurements were performed in the fore portion of the LSB using hot-wire anemometry, and in the after of the LSB using tomographic particle image velocimetry.

From the HWA measurements, small amplitude disturbances at the frequency of the LSB's primary Kelvin-Helmholtz instability were identified upstream of the LSB, which underwent convective amplification downstream of the mean separation point. When forced at this fundamental frequency in a two-dimensional manner, disturbance growth was almost entirely confined to the normal (2D) mode. When spanwise modulated forcing was applied, a distinct spanwise mode emerged in the disturbance profile, which was also convectively amplified. These findings point to the flow's instability to both normal and oblique disturbance waves, which can superimpose to form the experimentally measured disturbance profiles. The small amplitude disturbances tracked through the fore portion of the LSB were found to manifest in the shear layer vortices, imparting a spanwise wavelength, if present, in the vortex filaments. This lead to significant dislocations developing across the span of the filaments, where the streamwise forward sections tilt up and away from the way, leading to further vortex stretching by the mean shear.

ACKNOWLEDGEMENTS

The authors gratefully acknowledge the Natural Sciences and Engineering Research Council of Canada for funding this work.

REFERENCES

Arcondoulis, E. J. G., Doolan, C. J., Zander, A. C. & Brooks, L. A. 2010 A review of trailing edge noise generated by airfoils at low to moderate Reynolds number. *Acoust. Aust.* **38** (3), 129–133.

Atkinson, C. & Soria, J. 2009 An efficient simultaneous reconstruction technique for tomographic particle image velocimetry. *Exp. Fluids* **47**, 553–568.

Carmichael, B. H. 1981 Low Reynolds number airfoil survey, volume 1. *Tech. Rep.* NASA-CR-165803-VOL-1. National Aeronuatics and Space Administration.

Craik, A. D. D. 1971 Non-linear resonant instability in boundary layers. *J. Fluid Mech.* **50** (02), 393–413.

Desquesnes, G., Terracol, M. & Sagaut, P. 2007 Numerical investigation of the tone noise mechanism over laminar airfoils. *J. Fluid Mech.* **591**, 155–182.

Dovgal, A. V., Kozlov, V. V. & Michalke, A. 1994 Laminar boundary layer separation: Instability and associated phenomena. *Prog. Aerosp. Sci.* **30**, 61–94.

Gaster, M. 1967 The Structure and Behaviour of Laminar Separation Bubbles. *Aeronaut. Res. Counc.* **RM 3595**.

Hunt, J. C. R., Wray, A. A. & Moin, P. 1988 Eddies, streams, and convergence zones in turbulent flows. *Cent. Turbul. Res. Rep. CTR-S88* .

Kurelek, J. W., Kotsonis, M. & Yarusevych, S. 2018 Transition in a separation bubble under tonal and broadband acoustic excitation. *J. Fluid Mech.* **853**, 1–36.

Kurelek, J. W., Kotsonis, M. & Yarusevych, S. 2023 Superposition of AC-DBD plasma actuator outputs for three-dimensional disturbance production in shear flows. *Exp Fluids* **64** (4), 84.

Marxen, O. & Henningson, D. S. 2011 The effect of small-amplitude convective disturbances on the size and bursting of a laminar separation bubble. *J. Fluid Mech.* **671**, 1–33.

Marxen, O., Lang, M., Rist, U. & Wagner, S. 2003 A Combined Experimental/Numerical Study of Unsteady Phenomena in a Laminar Separation Bubble. *Flow Turbul. Combust.* **71** (1-4), 133–146.

Marxen, O., Rist, U. & Wagner, S. 2004 Effect of Spanwise-Modulated Disturbances on Transition in a Separated Boundary Layer. *AIAA J.* **42** (5), 937–944.

Michalke, A. 1964 On the inviscid instability of the hyperbolic-tangent velocity profile. *J. Fluid Mech.* **19** (04), 543–556.

Michelis, T., Yarusevych, S. & Kotsonis, M. 2018 On the origin of spanwise vortex deformations in laminar separation bubbles. *J. Fluid Mech.* **841**, 81–108.

O'Meara, M. & Mueller, T. J. 1987 Laminar separation bubble characteristics on an airfoil at low Reynolds numbers. *AIAA J.* **25** (8), 1033–1041.

Rist, U. & Augustin, K. 2006 Control of Laminar Separation Bubbles Using Instability Waves. *AIAA J.* **44** (10), 2217–2223.

Wieneke, B. 2008 Volume self-calibration for 3D particle image velocimetry. *Exp. Fluids* **45**, 549–556.

Yarusevych, S. & Kotsonis, M. 2017 Steady and transient response of a laminar separation bubble to controlled disturbances. *J. Fluid Mech.* **813**, 955–990.

Zelman, M. B. & Maslennikova, I. I. 1993 Tollmien-Schlichting-wave resonant mechanism for subharmonic-type transition. *J. Fluid Mech.* **252**, 449.